48th AIAA Aerospace Sciences Meeting Including the New Horizons Forum and Aerospace Exposition
4 - 7 January 2010, Orlando, Florida

Partition Design and Optimization for High-Order Spectral Volume Schemes on Tetrahedral Grids

Rob Harris*
CFD Research Corporation, Huntsville, AL 35805

Z. J. Wang†
Department of Aerospace Engineering, Iowa State University, Ames, IA 50011

An analysis of the accuracy and stability properties of the 3D spectral volume method on tetrahedral grids is presented. In the SV method, each simplex grid cell is called a spectral volume (SV), and the SV is further partitioned into polyhedral (3D) control volumes (CVs) to support high-order data reconstructions. In general, the partitioning of an SV into CVs is not uniquely defined, and thus it is of great importance to select a partition which yields favorable stability properties, and results in an interpolation polynomial of high quality. Here we present an approach to efficiently locate stable partitions by means of constrained minimization. This is motivated by the fact that, at present, an exhaustive search approach to SV partition design would be prohibitively costly and thus not feasible. Once stable partitions are located, a high quality interpolation polynomial is then assured by subsequently minimizing the dissipation and dispersion errors of the stable partitions. Results presented demonstrate the potential of this method for significantly reducing the strength of the weak instability currently present in the 3rd order scheme, and possibly even removing it completely.

I. Introduction

The spectral volume (SV) method is a recently developed finite volume method for hyperbolic conservation laws on unstructured grids.[1, 2, 3, 4, 5, 6, 7] The SV method belongs to a general class of Godunov-type finite volume method,[8, 9] which has been under development for several decades, and is considered to be the current state-of-the-art for the numerical solution of hyperbolic conservation laws. For a more detailed review of the literature on the Godunov-type method, refer to Wang,[1] and the references therein. Many of the most popular numerical methods, such as the k-exact finite volume,[10, 11] the essentially non-oscillatory (ENO),[12, 13] and weighted ENO[14] methods are also Godunov-type methods. A thorough review and comparison of these methods can be found in Wang.[15] The SV method is also closely related to the discontinuous Galerkin (DG)[16, 17, 18, 19, 20] method, a popular finite-element method for conservation laws. Both the SV and DG methods employ multiple degrees of freedom within a single element, but the SV method avoids the volume integral required in the DG method. Each simplex in the SV method utilizes a "structured" set of sub-cells, or control volumes (CVs), to support a polynomial reconstruction for the conserved variables, and a nodal set to support a polynomial reconstruction for the flux vector. For a more thorough comparison of the SV and DG methods, refer to Wang.[1, 15]

The partitioning of an SV into CVs has been one of the greatest challenges in the implementation of the SV method since its inception. This partitioning defines the reconstruction stencil, and thus plays a vital role in determining the accuracy and stability properties of the scheme. Early on, several researchers focused on using the Lebesgue constant as a means to design accurate SV partitions. In particular, the work of Wang,[2] Liu,[5] and Chen[21, 22] is of relevance. While this criteria may be used to find partitions with lower error bounds, it does not guarantee that a particular scheme will be more or less accurate, and it offers no information about the stability of the scheme. A positive step towards addressing the issue of stability was given by Van den Abeele et al.[23, 24, 25] In this work, some previously used SV partitions were found to be weakly unstable, and several new stable partitions were proposed. It was also shown that the new partitions

*Project Engineer, Aerospace & Defense Division, 215 Wynn Drive, reh@cfdrc.com, AIAA Member.
†Professor of Aerospace Engineering, 2271 Howe Hall, zjw@iastate.edu, Associate Fellow of AIAA.

had lower dissipation and dispersion errors than some previously used partitions despite having larger Lebesgue constants. This showed that although the Lebesgue constant should be small to ensure a lower upper bound on the error, it need not be minimal for a scheme to possess superior accuracy.

This paper is organized as follows. In Section 2, we review the basic formulation of the SV method. After that, the framework for stability analysis of the SV method on tetrahedral grids is described in detail in Section 3. Next, the methodology for partition design and optimization is outlined in Section 4. Results for optimization and numerical validation studies are then given in Section 5. Finally, conclusions are summarized in Section 6.

II. Review of the spectral volume method

Consider the multidimensional conservation law

$$\frac{\partial Q}{\partial t}+\frac{\partial f(Q)}{\partial x}+\frac{\partial g(Q)}{\partial y}+\frac{\partial h(Q)}{\partial z}=0, \tag{1}$$

on domain $\Omega \times [0,T]$ and $\Omega \subset R^3$ with the initial condition

$$Q(x,y,z,0)=Q_0(x,y,z), \tag{2}$$

and appropriate boundary conditions on $\partial\Omega$. In Eq. (1), x, y, and z are the Cartesian coordinates and $(x,y,z) \in \Omega$, $t \in [0,T]$ denotes time, Q is the vector of conserved variables, and f, g and h are the fluxes in the x, y and z directions, respectively. Domain Ω is discretized into I non-overlapping triangular (2D), or tetrahedral (3D) cells. In the SV method, the simplex grid cells are called SVs, denoted S_i, which are further partitioned into CVs, denoted $C_{i,j}$, which depend on the degree of the polynomial reconstruction. Volume-averaged conserved variables on the CVs are then used to reconstruct a high-order polynomial inside the SV. To represent the solution as a polynomial of degree m, we need N pieces of independent information, or degrees of freedom (DOFs). Where N is calculated as follows:

$$N=\frac{(m+1)(m+2)\cdots(m+d)}{d!}, \tag{3}$$

where d is the spatial dimension of the problem. The DOFs in the SV method are the volume-averaged conserved variables at the N CVs. Define the CV-averaged conserved variable for $C_{i,j}$ as

$$\overline{Q}_{i,j}=\frac{1}{V_{i,j}}\int_{C_{i,j}} Q\,dV, \quad j=1,\ldots,N, \quad i=1,\ldots,I, \tag{4}$$

where $V_{i,j}$ is the volume of $C_{i,j}$. Given the CV-averaged conserved variables for all CVs in S_i, a polynomial $p_i(x,y,z) \in P^m$ (the space of polynomials of at most degree m) can be reconstructed such that it is a $(m+1)^{\text{th}}$ order accurate approximation to $Q(x,y,z)$ inside S_i.

$$p_i(x,y,z)=Q(x,y,z)+O\left(h^{m+1}\right), \quad (x,y,z)\in S_i, \quad i=1,\ldots,I, \tag{5}$$

where h is the maximum edge length of all the CVs. This reconstruction can be solved analytically by satisfying the following condition:

$$\frac{1}{V_{i,j}}\int_{C_{i,j}} p_i(x,y,z)\,dV=\overline{Q}_{i,j}, \quad j=1,\ldots..,N. \tag{6}$$

This polynomial $p_i(x,y,z)$ is the $(m+1)^{th}$ order approximation we are looking for as long as the solution $Q(x,y,z)$ is smooth in the region covered by S_i. The reconstruction can be expressed more conveniently as

$$p_i(x,y,z)=\sum_{j=1}^{N} L_j(x,y,z)\overline{Q}_{i,j}, \tag{7}$$

where $L_j(x,y,z) \in P^m$ are the shape functions which satisfy

$$\frac{1}{V_{i,j}}\int_{C_{i,j}} L_n(x,y,z)\,dV=\delta_{jn}. \tag{8}$$

Integrating Eq. (1) in $C_{i,j}$, we obtain

$$\frac{d\overline{Q}_{i,j}}{dt}+\frac{1}{V_{i,j}}\sum_{r=1}^{K}\int_{A_r}\left(\vec{F}\cdot\vec{n}\right)dA=0, \qquad j=1,\ldots,N, \qquad i=1,\ldots,I, \tag{9}$$

where $\vec{F}=(f,g,h)$, A_r represents the r^{th} face of $C_{i,j}$, $\vec{n}$ is the outward unit normal vector of A_r, and K is the number of faces in $C_{i,j}$. More details of this, including representative plots of the shape functions can be found in Wang.[2] The integral in Eq. (9) can be computed using Gauss quadrature, or using the quadrature-

free approach outlined in Harris et al.[7] For time integration, we use either the 2nd- or 3rd-order SSP Runge-Kutta scheme from Gottlieb et al.[26] Some recent accomplishments in the development and application of the SV method can be found in Harris and Wang[27] and the references therein.

It was shown in Wang and Liu[2] that the so-called Lebesgue constant computed as

$$\left\|\Gamma_{\Pi}\right\| = \max_{\xi,\eta} \sum_{j=1}^{N} \left|L_j(\xi,\eta)\right|, \tag{10}$$

gives a simple method of bounding the interpolation polynomial for the SV method. Thus the smaller the Lebesgue constant $\left\|\Gamma_{\Pi}\right\|$, the better the interpolation polynomial in terms of error bounds. However, although this criteria can be helpful in finding accurate SV partitions, it carries no information about the stability properties of the resulting scheme, and is thus a necessary but not sufficient tool for designing SV partitions.

III. Formulation for stability analysis

The wave propagation properties associated with a particular SV partition and Riemann flux carry information about both the accuracy and stability of the numerical scheme. Recent work by Van den Abeele et al.[23, 24, 25] has utilized the so-called Fourier footprint to facilitate the design of stable SV partitions with favorable wave propagation properties. A similar analysis is employed here, with the distinction that here we couple the analysis with a constrained minimization procedure to intelligently locate stable and accurate partitions.

Consider the 3D linear advection equation

$$\frac{\partial Q}{\partial t} + \nabla \cdot (\vec{a} Q) = 0, \tag{11}$$

with periodic boundary conditions, where $\vec{a} = a(\sin\varphi\cos\psi,\ \sin\varphi\sin\psi,\ \cos\varphi)$ is the wave propagation velocity, ψ and φ are the wave propagation angles measured counterclockwise from the positive x-axis and down from the positive z-axis, respectively. The initial solution is taken to be a harmonic plane wave

$$Q(x,y,0) = e^{ik(x\cos\theta + y\sin\theta)}, \tag{12}$$

with wave number k and orientation angle θ. SV method is then applied to Eq. (11) on a grid comprised of hexahedral cells which have each been subdivided into six tetrahedral cells. The simplest unit which produces the entire grid when periodically repeated, commonly referred to as the generating pattern (GP), is shown in Figure 1.

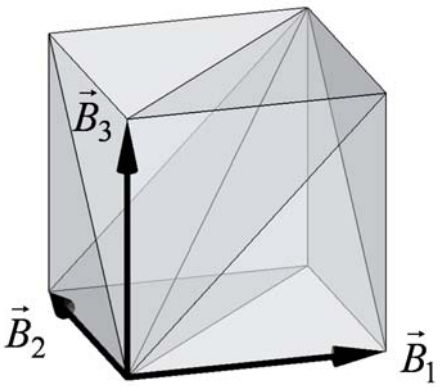

Figure 1. Generating pattern for regular tetrahedral grid.

The GP contains 6 SVs and is completely defined by the vectors $\vec{B}_1$, $\vec{B}_2$, and $\vec{B}_3$. The choice of 6 SVs in the GP rather than 5 facilitates the solution of a periodic problem by avoiding a face mismatch. On the boundary between the SVs, the following Riemann flux is employed

$$\hat{F}(Q_L, Q_R) = \frac{1}{2}\left(\vec{a}\cdot\vec{n} + \varphi\left|\vec{a}\cdot\vec{n}\right|\right)Q_L + \frac{1}{2}\left(\vec{a}\cdot\vec{n} - \varphi\left|\vec{a}\cdot\vec{n}\right|\right)Q_R, \tag{13}$$

where Q_L is the solution due to the SV to the left of the face, Q_R is the solution due to the SV to the right of the face, and φ is an upwinding parameter, where $\varphi = 0$ gives rise to a central flux, and $\varphi = 1$ results in a simple upwind flux. After applying the SV method to Eq. (11), we obtain

$$\sum_{n=1}^{6N}\left[\frac{V'\Delta B}{a}U_{m,n}\frac{d\overline{Q}_{i,j,k;n}}{dt}+M^{0}_{m,n}\overline{Q}_{i,j,k;n}+M^{-1}_{m,n}\overline{Q}_{i-1,j,k;n}+M^{+1}_{m,n}\overline{Q}_{i+1,j,k;n}\right.$$
$$\left.+N^{-1}_{m,n}\overline{Q}_{i,j-1;n}+N^{+1}_{m,n}\overline{Q}_{i,j+1;n}+O^{-1}_{m,n}\overline{Q}_{i,j,k-1;n}+O^{+1}_{m,n}\overline{Q}_{i,j,k+1;n}\right]=0\,, \qquad (14)$$

where ΔB is the magnitude of $\vec{B}_1$, a is the magnitude of $\vec{a}$, V' is the volume of an SV nondimensionalized by ΔB^2, the index m varies from 1 to $6N$, and the indices i, j and k are standard Cartesian indices to denote a particular GP in the grid. The variables $\overline{Q}_{i,j,k;n}$ for n = 1 to $6N$ are the CV-averages for all SVs in the generating pattern and the matrices $U_{m,n}$, $M^{0}_{m,n}$, $M^{-1}_{m,n}$, $M^{+1}_{m,n}$, $N^{-1}_{m,n}$, $N^{+1}_{m,n}$, $O^{-1}_{m,n}$, and $O^{+1}_{m,n}$ are functions of the wave propagation direction. Substitution of the harmonic plane wave $\overline{Q}_{i,j,k;m}(t)=\widetilde{Q}_m e^{i\left[k\left(\left(iB_{1x}+jB_{2x}+kB_{3x}\right)\cos\theta+\left(iB_{1y}+jB_{2y}+kB_{3y}\right)\sin\theta\right)-\omega t\right]}$ into Eq. (14) yields

$$\sum_{n=1}^{6N}\left[-i\widetilde{\Omega}V'U_{m,n}+M^{0}_{m,n}+M^{-1}_{m,n}e^{-iK\left(B'_{1x}\cos\theta+B'_{1y}\sin\theta\right)}+M^{+1}_{m,n}e^{+iK\left(B'_{1x}\cos\theta+B'_{1y}\sin\theta\right)}+N^{-1}_{m,n}e^{-iK\left(B'_{2x}\cos\theta+B'_{2y}\sin\theta\right)}\right.$$
$$\left.+N^{+1}_{m,n}e^{+iK\left(B'_{2x}\cos\theta+B'_{2y}\sin\theta\right)}+O^{-1}_{m,n}e^{-iK\left(B'_{3x}\cos\theta+B'_{3y}\sin\theta\right)}+O^{+1}_{m,n}e^{+iK\left(B'_{3x}\cos\theta+B'_{3y}\sin\theta\right)}\right]\widetilde{Q}_n=0\,, \qquad (15)$$

where K is the nondimensional wave number, the primed quantities denote non-dimensionalization by ΔB, and $\widetilde{\Omega}$ is the nondimensional numerical frequency. The numerical dispersion relation can then be written as

$$\left|-i\widetilde{\Omega}V'\mathbf{U}+\mathbf{M}^{o}+\mathbf{M}^{-1}e^{-iK\left(B'_{1x}\cos\theta+B'_{1y}\sin\theta\right)}+\mathbf{M}^{+1}e^{+iK\left(B'_{1x}\cos\theta+B'_{1y}\sin\theta\right)}+\mathbf{N}^{-1}e^{-iK\left(B'_{2x}\cos\theta+B'_{2y}\sin\theta\right)}\right.$$
$$\left.+\mathbf{N}^{+1}e^{+iK\left(B'_{2x}\cos\theta+B'_{2y}\sin\theta\right)}+\mathbf{O}^{-1}e^{+iK\left(B'_{3x}\cos\theta+B'_{3y}\sin\theta\right)}+\mathbf{O}^{+1}e^{+iK\left(B'_{3x}\cos\theta+B'_{3y}\sin\theta\right)}\right|=0\,, \qquad (16)$$

from which $\widetilde{\Omega}$ can be readily computed. The quantity $-i\widetilde{\Omega}$ is the so-called Fourier footprint $\Re=\Re^{\mathrm{Re}}+i\Re^{\mathrm{Im}}$ of the discretization, $\Re^{\mathrm{Im}}$ being a measure of the dispersive properties of the scheme, and $\Re^{\mathrm{Re}}$ being a measure of the diffusive properties. To ensure stability, $\Re^{\mathrm{Re}}$ should be nonpositive for all K, θ, and ψ.

IV. Partition design and optimization

The families of SV partitions considered here are inspired by the partitions presented in Chen.[22] Figure 2a shows a partition from Chen[22] supporting a 3rd-order scheme. We use this partition for the basic definition of the topology of the SV. There are 2 parameters that uniquely define the 3rd-order partition shown in Figure 2a. Essentially, these are two of the node locations for an internal quadrilateral face of the corner hexahedral CV. The remainder of the node locations are computed based on symmetry and the requirement that the nodes defining a face remain co-planar. Additionally, for a more general 3 parameter SV, we can subdivide the internal quadrilateral faces of the hexahedral cells into triangles, as shown in Figure 2b and 2c, and the co-planar face requirement is automatically satisfied. For clarity, a close-up view of all three of the aforementioned partitions is shown in Figure 3. The stability properties of these partitions will be addressed in the following section.

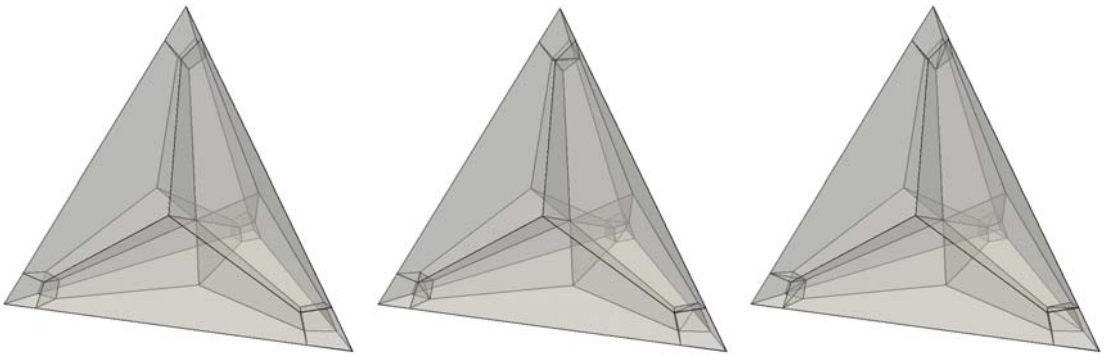

(a) (b) (c)

Figure 2. 3rd-order partitions of an SV used for definition of basic topology for optimization. (a) Original partition from Chen[22]; (b), (c) Partitions created by subdividing the hexahedral corner CVs into triangles in either direction.

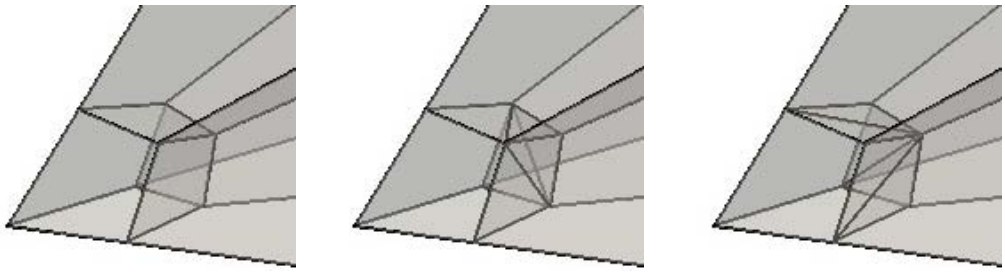

(a) (b) (c)

Figure 3. Close-up view of partitions shown in Figure 2. Internal faces of hexahedral corner CVs are quadrilaterals in (a) but split into triangles in (b) and (c).

An automated procedure has been developed to inspect the CV-partitioning of a tetrahedron and determine the minimum number of parameters that can be used to uniquely describe the partition. Once this information has been obtained, the constrained minimization program called CONMIN[28] is employed to optimize the SV partitions. CONMIN is a gradient-based optimizer which utilizes the method of Feasible Directions[29] to find the Feasible Direction, and then move in that direction to update the control parameters. The objective or cost function for CONMIN is taken to be the maximum real part of the Fourier footprint of the scheme $\Re^{\mathrm{Re}}_{\max}$. Since CONMIN is used for minimization, it will attempt to drive $\Re^{\mathrm{Re}}_{\max}$ to as low a value as possible by manipulating the parameters that define the partition, and if it reaches a nonpositive value, a stable partition has been discovered. Then, upon discovery of many stable partitions, those with the lowest dissipation and dispersion errors are deemed likely to be suitable for simulation.

V. Results

Optimization of 3rd order partition using constrained minimization

The constrained minimization approach outlined above is now applied to the 3rd order partitions shown in Figure 2. The Fourier footprint for the initial partition is shown in Figure 4, and t is apparent that the initial partition has a very small positive real part, which indicates that it suffers from a weak instability.

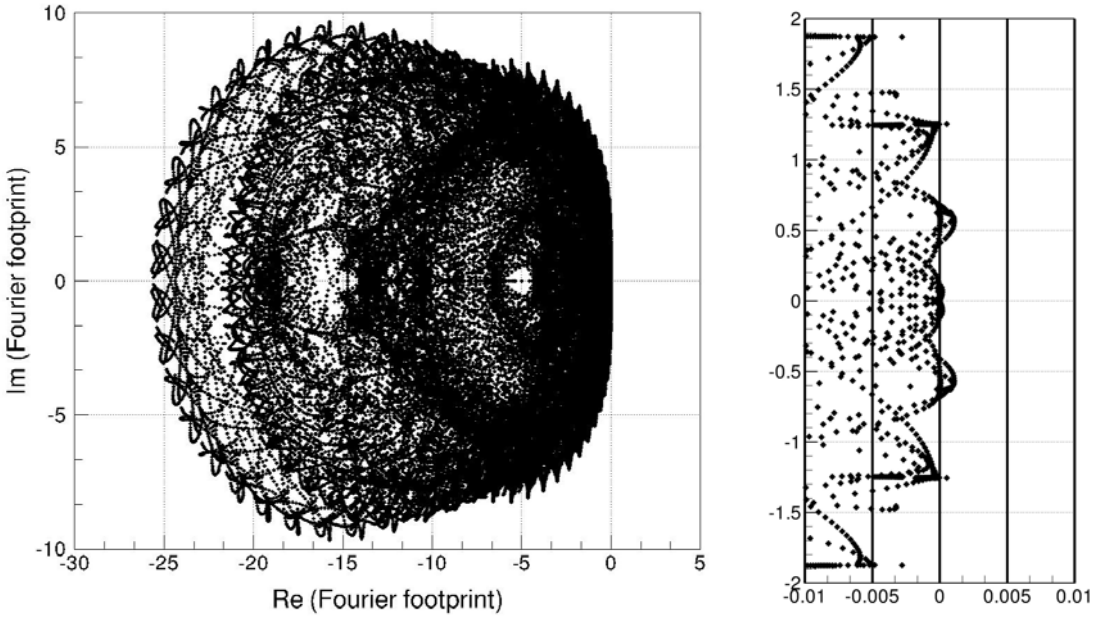

Figure 4. Fourier footprint for initial 3rd order partition shown in Figure 2a (left); Close-up view to illustrate weak instability (right).

Hundreds of different initial guess values for the parameters that define the partitions were employed to gain confidence into whether a local or global minimum is discovered. Thus far, several different partitions have been discovered with smaller maximum real Fourier footprint values over the original partition. The new partitions are shown in Figures 5-6 and are denoted as H1, H2, H3, and H4. The Fourier footprints for these cases are shown in Figures 7-8. While it is difficult to tell from the plots, the max real part of the Fourier footprint for partitions H1-H4 has been reduced by 10-20% from the initial value. The analytical results presented here will be verified in the following section by a series of numerical tests.

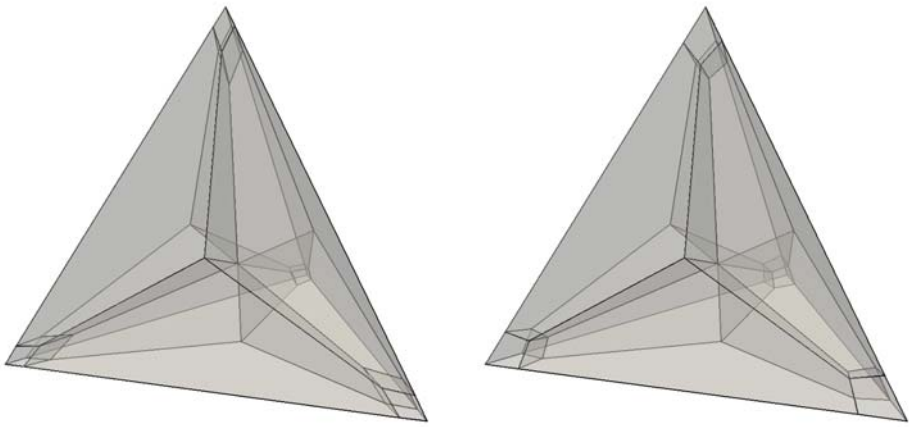

(a) **(b)**

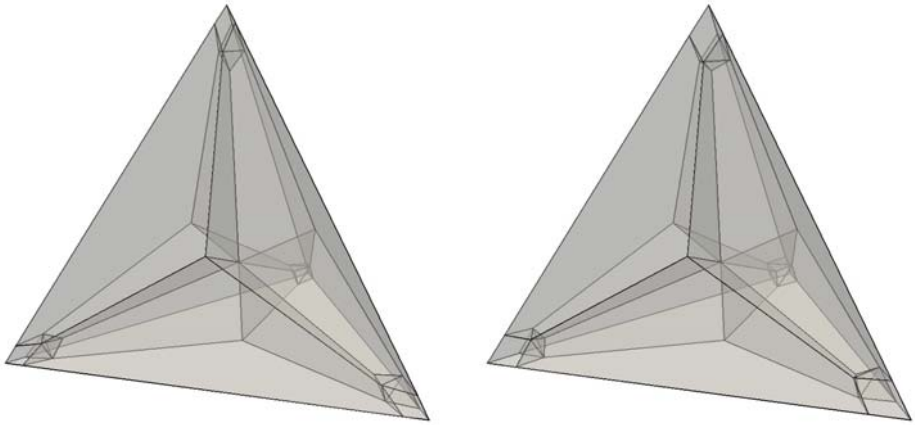

(c) **(d)**

Figure 5. Partitions resulting from optimization that give rise to weaker instabilities; Denote partitions as (a) H1; (b) H2; (c) H3; (d) H4.

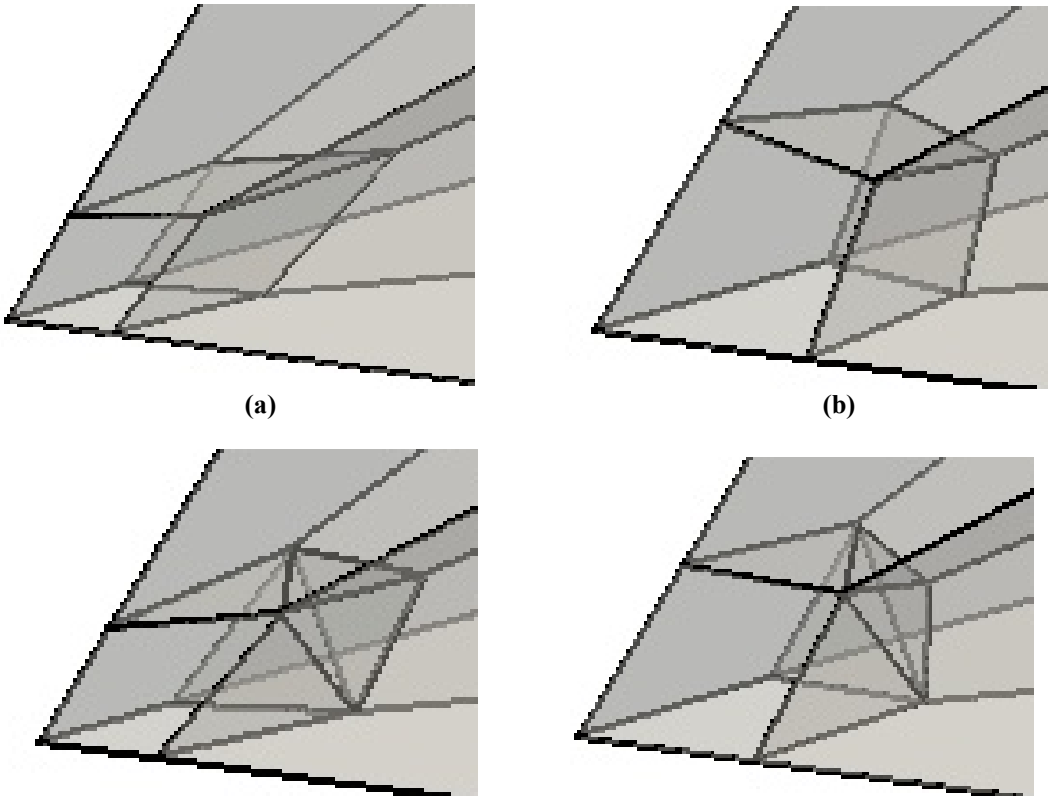

(a) **(b)**

(c) **(d)**

Figure 6. Close-up view of partitions shown in Figure 5.

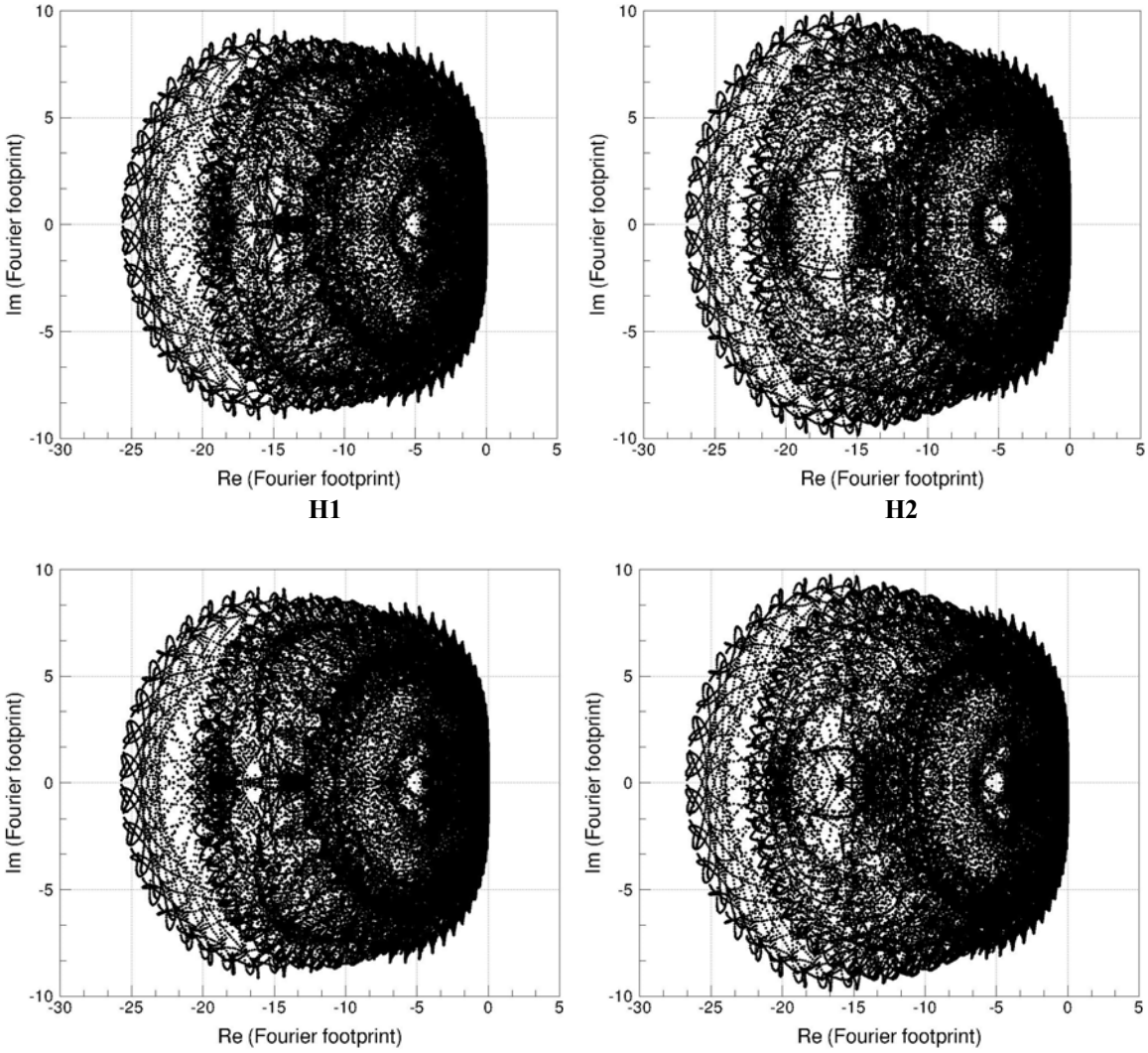

Figure 7. Fourier footprints for partitions shown in Figure 5.

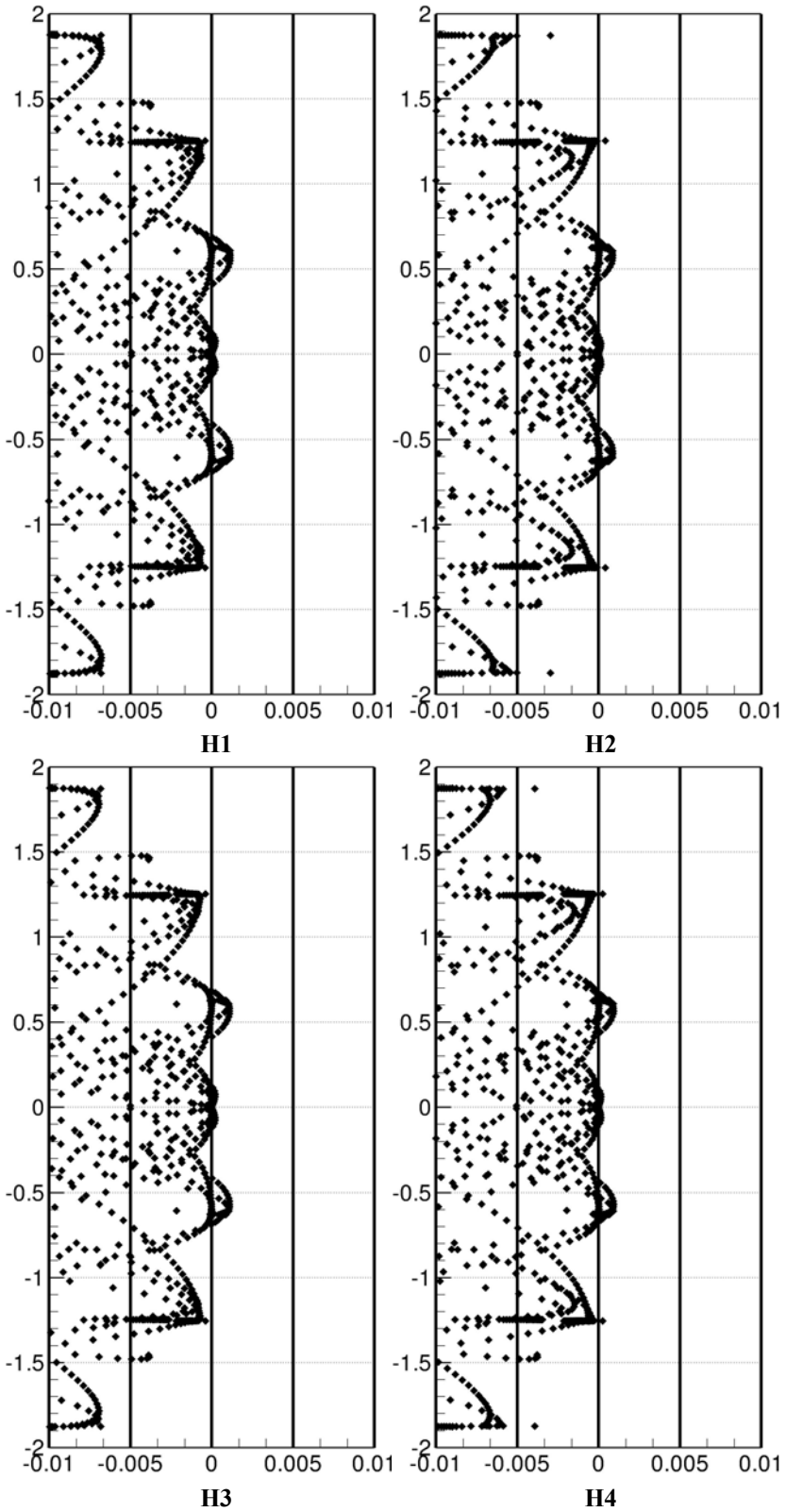

Figure 8. Close-up view of Fourier footprints shown in Figure 7.

Linear advection of a Gaussian pulse

To numerically verify improvements in the stability properties obtained in the previous section, the linear advection of a Gaussian pulse is considered. The equation to be solved is Eq. (11), and the initial solution is taken to be a Gaussian pulse with a half-width of 1/10 given as follows:

$$Q_0(x,y) = \exp\left(-\frac{(x-x_0)^2+(y-y_0)^2}{r_0^2}\right), \quad r_0 = 1/10 \tag{17}$$

The coordinates x_0 and y_0 are the initial position of the maximum of the pulse. The numerical solution is carried out on grids comprised entirely of cubes, each split into 6 tetrahedral SVs. An upwind Riemann solver is used for the convective fluxes, and for time integration we use the 3rd order Strong Stability-Preserving (SSP) Runge-Kutta scheme.[26] The computational grid and initial solution used for this problem is shown in Figure 9. The grid contains 600 cells and periodic boundary conditions are assumed on all sides of the domain so as to avoid any additional errors due to implementation of numerical boundary conditions. Two different wave speeds, $\vec{a} = (1,0)$ and $\vec{a} = (1,1)$, are considered here and the pulse is allowed to convect until the instability is sufficiently observed by monitoring the L_2 norm of the residual.

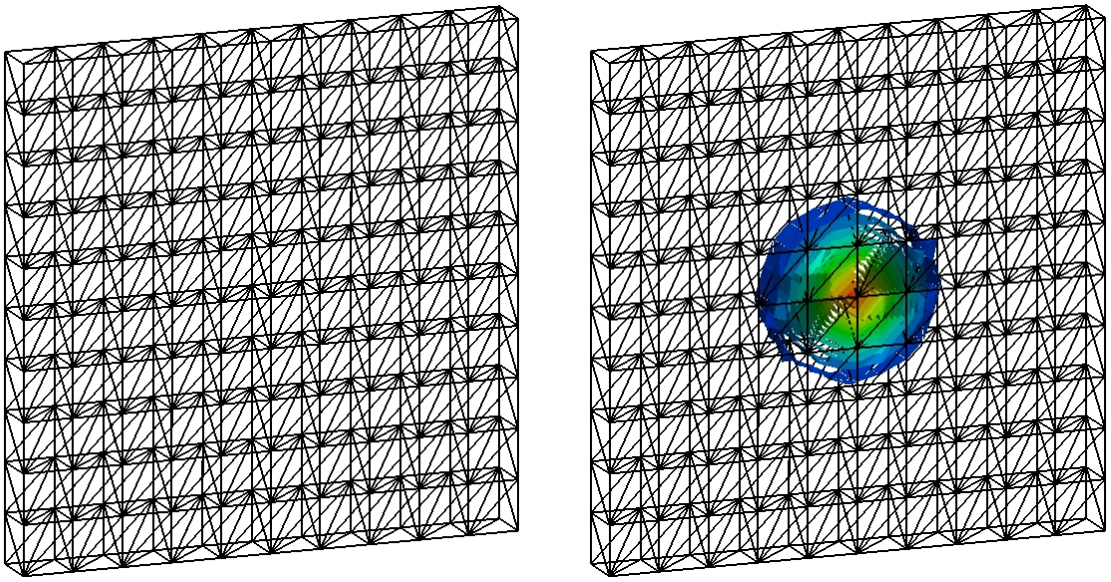

Figure 9. Grid (left) and Grid with initial contours (right) for Gaussian pulse case (600 SVs).

The residual histories for this case are shown in Figure 10. Results for the partition from Chen[22] and the optimized partitions H1-H4 shown in Figure 5 are displayed for comparison purposes. The weak instability is apparent for all cases, so the optimization process has not been able to completely stabilize the scheme at present. However, the optimization process has resulted in a dramatic weakening of the instability by about an order-of-magnitude for some cases. For example, the results for the H4 partition at zero wave angle demonstrate that the instability is not triggered until almost 300,000 iterations have been carried out, compared to only 30,000 iterations for the original partition before optimization.

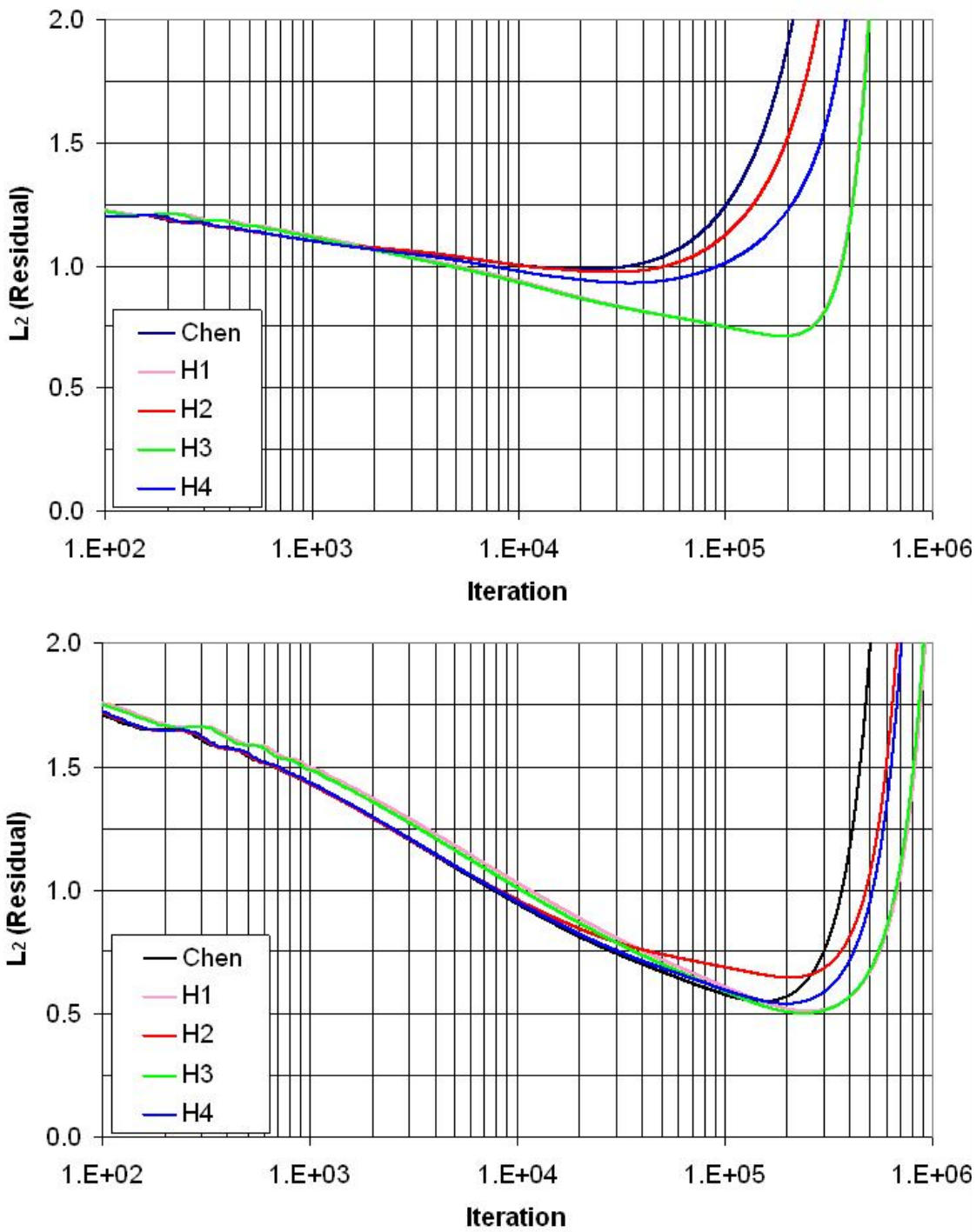

Figure 10. Residual history for Gaussian pulse case using partitions shown in Figures 2a and 5: (top) wave angle = 0; (bottom) wave angle = π/4.

VI. Conclusions

The constrained minimization approach has been applied in the design of 3D 3rd-order spectral volume schemes with improved stability properties. Several new partitions were presented which have a reduced maximum real part of the Fourier footprint by up to 20% over the original un-optimized partition. Numerical simulation of the convection of a Gaussian pulse was employed to numerically verify the analytical results, and it was shown that the strength of the instability was weakened by about an order-of-magnitude for some cases by employing the constrained minimization approach. While the instability is still observed in the 3D 3rd-order scheme, it has been significantly weakened and is less of an issue now. Extension of the optimization procedure to include different types of objective functions and constraints, as well as possible use of a global optimization strategy is of future interest.

Acknowledgements

This study has been partially supported by the Air Force Office of Scientific Research (AFOSR) and the Department of Energy (DOE). The views and conclusions contained herein are those of the authors and should not be interpreted as necessarily representing the official policies or endorsements, either expressed or implied, of the AFOSR and DOE.

References

[1] Z. J. Wang, Spectral (finite) volume method for conservation laws on unstructured grids: basic formulation, J. Comput. Phys. 178 (2002) 210.

[2] Z. J. Wang, Y. Liu, Spectral (finite) volume method for conservation laws on unstructured grids II: extension to two-dimensional scalar equation, J. Comput. Phys. 179 (2002) 665.

[3] Z. J. Wang, Y. Liu, Spectral (finite) volume method for conservation laws on unstructured grids III: extension to one-dimensional systems, J. Sci. Comput. 20 (2004) 137.

[4] Z. J. Wang, Y. Liu, Spectral (finite) volume method for conservation laws on unstructured grids IV: extension to two-dimensional Euler equations, J. Comput. Phys. 194 (2004) 716.

[5] Y. Liu, M. Vinokur, Z. J. Wang, Spectral (finite) volume method for conservation laws on unstructured grids V: extension to three-dimensional systems, J. Comput. Phys. 212 (2006) 454-472.

[6] Y. Sun, Z. J. Wang, Y. Liu, Spectral (finite) volume method for conservation laws on unstructured grids VI: extension to viscous flow, J. Comput. Phys. 215 (2006) 41-58.

[7] R. Harris, Z. J. Wang, Y. Liu, Efficient quadrature-free high-order spectral volume method on unstructured grids: Theory and 2D implementation, J. Comput. Phys. 227 (2008) 1620-1642.

[8] S. K. Godunov, A finite-difference method for the numerical computation of discontinuous solutions of the equations of fluid dynamics, Mat. Sb. 47 (1959) 271.

[9] B. van Leer, Towards the ultimate conservative difference scheme V. a second-order sequel to Godunov's method, J. Comput. Phys. 32 (1979) 101-136.

[10] T. J. Barth, P.O. Frederickson, High-order solution of the Euler equations on unstructured grids using quadratic reconstruction, AIAA Paper No. 90-0013, 1990.

[11] M. Delanaye, Yen Liu, Quadratic reconstruction finite volume schemes on 3D arbitrary unstructured polyhedral grids, AIAA Paper No. 99-3259-CP, 1999.

[12] A. Harten, B. Engquist, S. Osher, S. Chakravarthy, Uniformly high order essentially non-oscillatory schemes III, J. Comput. Phys. 71 (1987) 231.

[13] R. Abgrall, On essentially non-oscillatory schemes on unstructured meshes: analysis and implementation, J. Comput. Phys. 114 (1994) 45-58.

[14] C. Hu, C.-W. Shu, Weighted essentially non-oscillatory schemes on triangular meshes, J. Comput. Phys. 150 (1999) 97-127.

[15] Z.J. Wang, High-Order Methods for the Euler and Navier-Stokes Equations on Unstructured Grids, Journal of Progress in Aerospace Sciences, Vol. 43 No. 1-3 (2007).

[16] B. Cockburn, C.-W. Shu, TVB Runge-Kutta local projection discontinuous Galerkin finite element method for conservation laws II: general framework, Math. Comput. 52 (1989) 411-435.

[17] B. Cockburn, S.-Y. Lin, C.-W. Shu, TVB Runge-Kutta local projection discontinuous Galerkin finite element method for conservation laws III: one-dimensional systems, J. Comput. Phys. 84 (1989) 90-113.

[18] B. Cockburn, S. Hou, C.-W. Shu, TVB Runge-Kutta local projection discontinuous Galerkin finite element method for conservation laws IV: the multidimensional case, Math. Comput. 54 (1990) 545-581.

[19] B. Cockburn, C.-W. Shu, The Runge-Kutta discontinuous Galerkin method for conservation laws V: multidimensional systems, J. Comput. Phys. 141 (1998) 199-224.
[20] H. L. Atkins, Chi-Wang Shu, Quadrature-free implementation of the discontinuous Galerkin method for hyperbolic equations, AIAA J. 96 (1996) 1683.
[21] Q.-Y. Chen, Partitions of a simplex leading to accurate spectral (finite) volume reconstruction. SIAM J. Sci. Comput. Vol. 27, No. 4 (2006) 1458-1470.
[22] Q.-Y. Chen, Partitions for spectral (finite) volume reconstruction in the tetrahedron, SIAM J. Sci. Comput. (2005).
[23] K. Van den Abeele, T. Broeckhoven, and C. Lacor, Dispersion and Dissipation properties of the 1D spectral volume method and application to a p-multigrid algorithm, J. Comput. Phys. 224 (2) (2007) 616-636.
[24] K. Van den Abeele, and C. Lacor, An accuracy and stability study of the 2D spectral volume method, J. Comput. Phys. 226 (1) (2007) 1007-1026.
[25] K. Van den Abeele, G. Ghorbaniasl, M. Parsani, and C. Lacor, A stability analysis for the spectral volume method on tetrahedral grids, J. comput. Phys. 228(2) (2009) 257-265.
[26] S. Gottlieb, C-W. Shu, E. Tadmor, Strong stability-preserving high-order time discretization methods, SIAM Review, v.43 n.1, p. 89-112, 2001.
[27] R. Harris and Z.J. Wang, High-Order Adaptive Quadrature-Free Spectral Volume Method on Unstructured Grids, Computers and Fluids, 38 (2009) 2006-2025.
[28] N. G. Vanderplaats, CONMIN USER'S MANUAL, Ames Research Center and U.S. Army Air Mobility, R&D Laboratory, Moffet Field, Calif. 94035, 1978.
[29] G. Zoutendijk, Methods of Feasible Directions, Elsevier Publishing Co., Amsterdam, 1960.